PNAS RESEARCH ARTICLE | PHYSICS

Stress-activated friction in sheared suspensions probed with piezoelectric nanoparticles

Hojin Kim[a,b,1], Aaron P. Esser-Kahn[a], Stuart J. Rowan[a,c,d,1], and Heinrich M. Jaeger[b,1]

Edited by David Weitz, Harvard University, Cambridge, MA; received June 15, 2023; accepted October 28, 2023

A hallmark of concentrated suspensions is non-Newtonian behavior, whereby the viscosity increases dramatically once a characteristic shear rate or stress is exceeded. Such strong shear thickening is thought to originate from a network of frictional particle–particle contact forces, which forms under sufficiently large stress, evolves dynamically, and adapts to changing loads. While there is much evidence from simulations for the emergence of this network during shear thickening, experimental confirmation has been difficult. Here, we use suspensions of piezoelectric nanoparticles and exploit the strong local stress focusing within the network to activate charge generation. This charging can then be detected in the measured ac conductance and serve as a signature of frictional contact formation. The direct link between stress-activated frictional particle interactions and piezoelectric suspension response is further demonstrated by tracking the emergence of structural memory in the contact network under oscillatory shear and by showing how stress-activated friction can drive mechano-transduction of chemical reactions with nonlinear reaction kinetics. Taken together, this makes the ac conductance of piezoelectric suspensions a sensitive in-situ reporter of the micromechanics associated with frictional interactions.

discontinuous shear thickening | frictional network | contact force | piezoelectricity

Shearing a concentrated, or dense, suspension of small particles in a simple liquid drives these particles into contact (1–4). For sufficiently large shear, simulations show that these contacts become frictional and form chains that organize into a network of branching paths along which most stress is transmitted (5, 6). Once this network of frictional contact forces extends throughout the suspension, it changes the overall behavior from easily flowing to nearly rigid, a striking transformation that is fully reversible. Such behaviour has led to these materials being explored in applications that include stress-adaptive materials for impact and penetration mitigation, vibration damping, or flow control (7–9). However, direct experimental evidence for the contact force network is hampered by the difficulty of detecting local particle–particle contacts inside a suspension.

Prior work on dense suspensions has explored particle configurations utilizing confocal microscopy imaging and extracting information from particle center-to-center spacings, either in flowing systems (1) or in suspensions arrested with a photocrosslinker (10). Related approaches have been used in emulsions (11) as well as assemblies of larger hydrogel particles (12). Direct extraction of local contact forces in an assembly's interior has only been possible in macroscopic dry granular packings of two-dimensional (2D) photoelastic particles (13, 14) and, in dry 3D packings, using magnetic resonance elastography (15) or combinations of x-ray diffraction and tomography together with numerical modeling (16).

Here, we introduce an approach that, simultaneously with measurement of the viscosity, monitors changes in the electrical conductance of a dense suspension of piezoelectric nanoparticles under shear (Fig. 1*A*). This does not give spatially localized information, but it can signal the emergence of frictional contact force networks with high sensitivity and it allows for in-situ measurements under shear.

When strained, piezoelectric particles develop an electric dipole moment that generates charges at the particle surface. Such particles, either as dense aggregates or embedded at low density in a suitable matrix, have found a range of applications, including as converters of mechanical energy into electric energy for energy harvesting (17, 18). Generally, to obtain a large response to strain from an assembly of spatially fixed, but randomly oriented piezoelectric particles, an initial poling step is applied during which a large electric field aligns the local dipole moments. In a sheared suspension, any effect of poling is negated since particles reconfigure and reorient continually, which keeps randomizing their polarization directions. Furthermore, piezoelectric particles are nonmetallic and their own contribution to the suspension conductivity at rest is typically very small. However, if they

Significance

The origin of the dramatic, non-Newtonian increase of the viscosity with increasing shear intensity in concentrated particle suspensions has long been debated. While earlier simulations identified fluid-mediated lubrication forces as responsible for such shear thickening, more recent simulations have pointed to the formation of a network of frictional particle–particle contacts. However, experimental confirmation of such frictional contacts is beset with technical difficulties. Here, we overcome this experimental challenge by using dense suspensions of piezoelectric nanoparticles and detecting the piezoelectricity induced by friction in measurements of the ac conductance. This makes it possible to detect with a bulk measurement the emergence of microscopic frictional contacts and correlate this with the onset of strong shear thickening.

Author contributions: H.K., S.J.R., and H.M.J. designed research; H.K. performed research; H.K., A.P.E.-K., S.J.R., and H.M.J. analyzed data; and H.K., A.P.E.-K., S.J.R., and H.M.J. wrote the paper.

The authors declare no competing interest.

This article is a PNAS Direct Submission.

[1]To whom correspondence may be addressed. Email: hojinkim718@gmail.com, stuartrowan@uchicago.edu, or jaeger@uchicago.edu.

This article contains supporting information online at https://www.pnas.org/lookup/suppl/doi:10.1073/pnas.2310088120/-/DCSupplemental.

Published November 28, 2023.

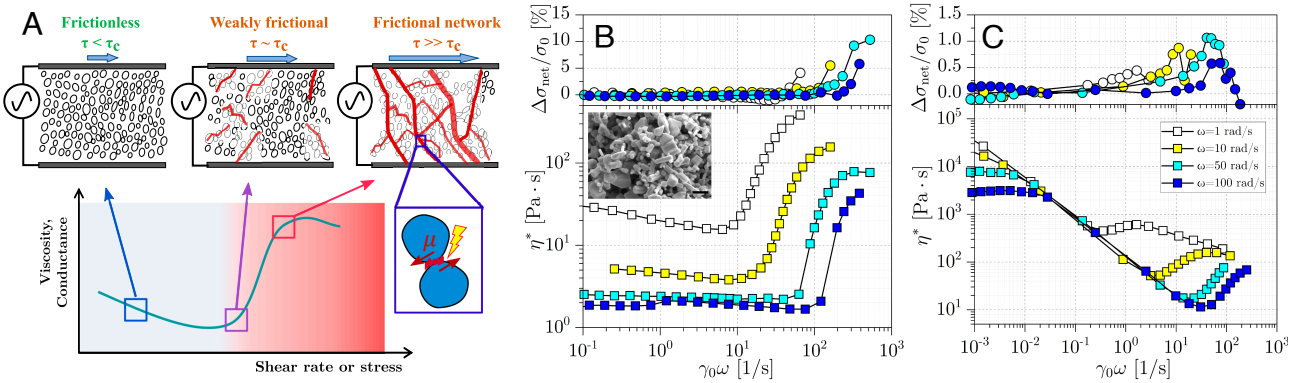

Fig. 1. Piezoelectricity signals emergence of frictional contact network in the shear thickening regime. (*A*) As a dense suspension of piezoelectric nanoparticles shear thickens due to a transition from frictionless (gray) to frictional (red) particle–particle interactions, friction-induced piezoelectricity in the contacting particles generates electric charge, which in turn increases the ac conductance of the surrounding fluid. (*B*) Complex viscosity η^* (*Bottom*) and normalized excess conductance $\Delta\sigma_{net}/\sigma_0$ (*Top*) under oscillatory shear as a function of dynamic shear rate $\gamma_0\omega$ for ZnO nanoparticles (*Inset* Scale bar, 500 nm). The particles are suspended in glycerol at volume fraction ϕ=0.36. Stress-controlled oscillatory shear is applied with angular frequencies $\omega = 1$ (white), 10 (yellow), 50 (cyan), and 100 rad/s (blue). (*C*) The same data as in (*B*) but for ZnO particles in glycerol with 100 mM of NaCl salt added, at volume fraction ϕ=0.33.

are suspended in an aqueous liquid of finite conductivity, the surface charges they produce when strained can transfer into the surrounding liquid through the Faradaic current (19). These charges lead to an increase in conductivity across the suspension. This process is independent of the individual particles' polarization direction while particles reorient under shear. It can be expected to become particularly efficient when particles are sheared into chain-like arrangements, as happens when contact force networks form during shear thickening. These networks tend to be anisotropic, oriented predominantly along the forward compressive direction, and are highly heterogeneous. As a result, during shear thickening, the uniformly applied stress at the boundaries is focused along a small number of force chains that carry the majority of the load (6). This stress focusing, whereby the local contact stress can largely exceed the average value, serves as an effective mechanism to enhance the piezoelectric response. Similar local stress enhancement has also been found in open-pore, network-type architectures of piezoelectric solids (17). Importantly, to generate an ac conductance signal no system-spanning, fully percolated networks are required. In our suspensions, the ac current is carried by the suspending liquid and not the particles, which are effectively nonconducting. Therefore, an observable increase in the ac conductance can be generated from particle–particle interactions anywhere in the suspension as long as they are strong enough to generate Faradaic current for our bulk conductance measurement to pick up. Thus, while the ac conductance by itself cannot be used to distinguish between different mechanisms producing the shear-induced large local stresses, such differentiation becomes possible in combination with simultaneous rheological measurements.

In the following, we first demonstrate how the emergence, and evolution, of frictional contact force networks during shear thickening in dense suspensions of piezoelectric particles can be tracked by measuring the suspension conductance (Fig. 1*A*). We show this with ZnO as well as $BaTiO_3$ nanoparticles for different volume fractions, suspending liquids, and oscillatory shearing conditions. We then show how the frictional, stress-activated piezoelectric response in such suspensions can serve to track structural memory in the contact force network and drive chemical reactions.

In our experiments, the piezoelectric particles are suspended in glycerol at different volume fractions ϕ. It is worthwhile noting that commercial particles used here have a wide distribution of shapes and sizes. However, while size dispersion tends to broaden the observed shear thickening, it does not eliminate it (20) and increased particle anisotropy tends to enhance shear thickening (21–23). The complex viscosity η^* is then measured under oscillatory shear (parallel plate geometry) as a function of dynamic shear rate $\gamma_0\omega$, whereby the shear strain amplitude γ_0 is increased while keeping the angular frequency ω fixed. Simultaneously the electrical ac conductance σ is measured by applying an alternating voltage (amplitude 1 V_{rms}, frequency 100 Hz) across the rheometer plates, which serve as electrodes (Fig. 1*A*). In order to track changes in conductance with dynamic shear rate, the background conductance σ_0 of the quiescent suspension is subtracted from σ (for raw conductance data, see *SI Appendix*, Figs. S1 and S2). In addition, the slow but steady increase of conductance with time, caused by charge buildup at the electrodes on account of Maxwell–Wagner polarization in the suspending liquid (24), is also subtracted. The remaining, shear-induced enhancement in ac conductance is then calculated as $\Delta\sigma_{net}/\sigma_0 = \left(\sigma - \sigma_0 - \frac{\partial\sigma}{\partial t}|_{t=0}\Delta t\right)/\sigma_0$, which is normalized by the background value σ_0. Here, $\frac{\partial\sigma}{\partial t}|_{t=0}$ is the rate of conductance change from Maxwell–Wagner polarization and Δt the measurement time interval. The effect of particle sedimentation in contributing to the measured $\Delta\sigma_{net}/\sigma_0$ is negligible given that the stress from particle weight is orders of magnitude lower than the stress where we first pick up a signal in the excess conductance, namely at the onset of strong shear thickening (see *Materials and Methods* for details).

Fig. 1*B* shows the complex viscosity η^* and excess ac conductance $\Delta\sigma_{net}/\sigma_0$ for a suspension of ZnO particles (average diameter $d \simeq 1$ μm) in glycerol at volume fraction $\phi = 0.36$. The rapid rise in η^* beyond some characteristic shear rate $\gamma_0\omega$ is a signature of pronounced, nearly discontinuous shear thickening associated with the onset of shear-induced, frictional interparticle contacts (5, 6). As the Fig. 1 *B*, *Top* shows, this rise in η^* is mirrored by a corresponding rise in $\Delta\sigma_{net}/\sigma_0$. At the same time, a shift in the onset for shear thickening to larger dynamic shear rates $\gamma_0\omega$ is observed in both η^* and $\Delta\sigma_{net}/\sigma_0$. This shift shows that the mechanism driving the thickening and the excess conductance is not tied to a specific, characteristic shear rate $\gamma_0\omega$, as would have been expected for fluid-mediated particle interactions, where the particles experience rate-dependent lubrication forces but no direct frictional contact (see, e.g., ref. 25). Instead, the shift is

a consequence of the condition that the stress $\tau = \eta^* \gamma_0 \omega$ has to reach a minimum critical magnitude τ_c in order to activate frictional particle–particle contacts, which, for larger ω, moves the onset to smaller viscosity (5, 6). In combination with the viscosity data, the increase in conductance can therefore be associated with a stress-induced transition from frictionless to frictional interactions inside the suspension.

To verify that the measured excess conductance is indeed associated with particle contact formation and not simply with the viscosity magnitude, we can alter the overall rheological behaviour of the suspension by adding salt to the suspending liquid (Fig. 1*C*). The salt screens the surface charges, lowering the electrostatic repulsion between particles. As a result, a strong shear thinning at low $\gamma_0 \omega$ is observed along with significant weakening of the degree of thickening under shear at larger $\gamma_0 \omega$, as seen in the less steep rise of η^* beyond the thickening onset. Concomitantly, the magnitude of $\Delta\sigma_{net}/\sigma_0$ is reduced by a factor 10. Importantly, $\Delta\sigma_{net}/\sigma_0$ in Fig. 1*C* shows a clear increase only around the point where shear thickening sets in.

At a salt concentration of [NaCl]$=$ 0.1 mol L^{-1}, as in Fig. 1*C*, the Debye length κ^{-1} of a ZnO particle in glycerol becomes sufficiently small (around 1 nm) that attractive short-range interactions generate particle agglomerates at rest, which then yield and break up under shear, leading to the observed pronounced shear thinning with increasing $\gamma_0 \omega$. Importantly, while these attractive forces stabilize the agglomerates, the particles are not sheared into contact, and therefore, no piezoelectric response is observed. Only once the applied stress is increased sufficiently is the piezoelectric response of the particles activated. This behavior differs from high-conductivity carbon black suspensions, where the particles themselves contribute significantly to the overall ac electrical conductivity, which generally drops with increasing shear rate (26). The absence of a piezoelectric response in silane-coated ZnO (27) or of changes in $\Delta\sigma_{net}/\sigma_0$ in fumed silica suspensions exhibiting significant shear thickening (*SI Appendix*, Fig. S3) further supports that the concurrent increase of viscosity and ac conductance originates from stress-induced piezoelectricity between particles.

A similar, direct correspondence between the onset of shear thickening and an increase in $\Delta\sigma_{net}/\sigma_0$ is found for barium titanate ($BaTiO_3$ or BTO) particles of average diameter $d = 500$ nm suspended in glycerol. Such BTO suspensions exhibit shear thinning at low shear rates even without the addition of salt. Since the piezoelectric constant is almost an order of magnitude larger in BTO compared to ZnO, this enables us to track the piezoelectric response in more detail in BTO suspensions with a smaller solid fraction. Decreasing the BTO particle volume fraction ϕ from 0.49 to 0.25 decreases the degree of both shear thinning and thickening, and with it the magnitude of $\Delta\sigma_{net}/\sigma_0$ in the thickening regime (Fig. 2*A*). However, even at $\phi = 0.25$, where there is only very weak apparent thickening, we can still detect a small increase in $\Delta\sigma_{net}/\sigma_0$ (Fig. 2*B*). Given that system-spanning contact networks are extremely unlikely to form at such low volume fraction, this serves as a reminder that the ac conductance does not rely on a fully percolated network and can detect sufficiently strong stress loading anywhere in a suspension of piezoelectric particles. As shown in Fig. 2 *B* and *C* for the $\phi = 0.25$ and $\phi = 0.49$ data (all intermediate concentrations are available in *SI Appendix*, Fig. S4), increasing ω from 1 rad/s to 100 rad/s increases the magnitude the $\Delta\sigma_{net}/\sigma_0$ signal.

Since shear thinning and shear thickening arise from different mechanisms and exhibit opposite trends as a function of $\gamma_0 \omega$, their contributions to the viscosity result in a crossover regime at intermediate shear rate, where thinning can mask the emerging thickening (21, 28). Close inspection of the data in Fig. 2 reveals that the excess conductance $\Delta\sigma_{net}/\sigma_0$ rises slightly before the viscosity minimum is reached. This is a further indication that the conductance signal is sensitive to the formation of the frictional force chain network, even in its early stages.

With regard to the apparent peak observed in much of the $\Delta\sigma_{net}/\sigma_0$ data in Figs. 1 and 2, it is important to note that oscillatory shear measurements at the highest shear rates in both the ZnO and BTO suspensions are difficult because of interfacial instabilities that can lead to radial ejection of material from the shear cell, and thus, the data beyond the maximum $\Delta\sigma_{net}/\sigma_0$ are less reliable. Nevertheless, the clear peak in the data for the largest packing fractions in Fig. 2*A* could indicate that there are structural changes in the force chain network before the transition into the fully shear-thickened, high-viscosity state has been completed. In particular, the peak could reflect the crossover from a sparser, more anisotropic network to a denser, more homogeneous and isotropic network structure, as found in granular systems (29) and simulations of suspensions

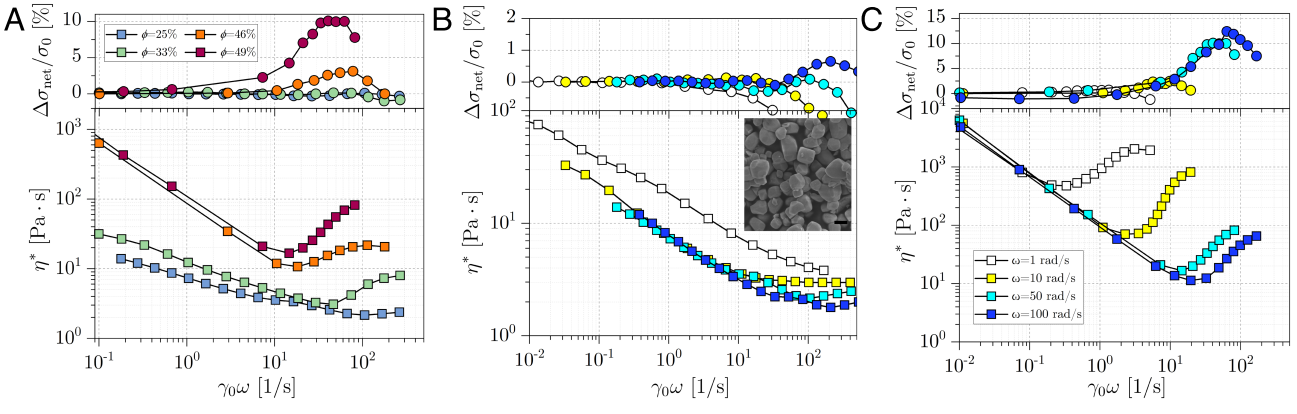

Fig. 2. Conductance measurements can track frictional contact network formation with high sensitivity. Data in this figure are for BTO nanoparticles. (*A*) $\Delta\sigma_{net}/\sigma_0$ and η^* for different BTO volume fractions ($\phi = 0.25$, blue; 0.33, green; 0.46, orange; 0.49, red) as function of dynamic shear rate $\gamma_0\omega$ at fixed shear oscillation frequency $\omega = 50$ rad s^{-1}. (*B* and *C*) Frequency dependence of η^* and $\Delta\sigma_{net}/\sigma_0$ for two of the volume fractions plotted in (*A*), namely ϕ=0.25 (*B*) and ϕ=0.49 (*C*) of BTO nanoparticles (see *Inset* to (*B*), Scale bar, 500 nm). The plots show data for oscillation frequencies $\omega = 1$ (white), 10 (yellow), 50 (cyan), and 100 rad/s (blue). With increasing frequency, the excess conductance becomes more sensitive and enables the detection of the onset of frictional contacts as a result of shear thickening even when that onset is obscured in the viscosity by residual shear thinning behavior.

(30). As the network becomes denser and the local connectivity increases quicker than the applied stress, forces become more evenly distributed and the amount of stress per contact decreases, resulting in a decrease in ac conductance.

The simultaneous measurement of viscosity and conductance in suspensions of piezoelectric particles provides special access to signatures of particle self-organization and strain-dependent memory associated with the evolution of the frictional force network over time. In studies of jammed and glassy colloidal and granular particle systems under oscillatory shear (31–34), it was found that repeated reversal of the shearing direction at given stress reinforces the most robust network configurations. Effectively, this trains the network to evolve toward the subset of configurations that, for given τ, are most efficient at quick rebuilding after each reversal of the shearing direction.

To observe this structural memory with a BTO suspension, oscillatory shear at constant stress τ is applied and η^* and σ are measured as a function of time. This stress is then increased in steps as shown in the Fig. 3 *A*, *Inset*. Following each increase in τ, the viscosity η^* jumps to a new, larger magnitude (Fig. 3*A*). After each jump, a hint of the network reconfiguration can already be seen in the small, but noticeable, decrease of the viscosity with time, especially at larger stresses (35). Since the applied stress is held constant in these experiments, this gradual reduction of η^* indicates a speedup of the dynamic shear rate, consistent with a more effective and thus faster reconfiguration during shear reversal. This small trend in η^* is mirrored, in a much more amplified fashion, in the excess conductance $\Delta\sigma_{\text{net}}/\sigma_0$ in Fig. 3*A*. Starting near the onset of shear thickening, at stress τ_1, the excess conductance is essentially independent of time. As the suspension reaches the middle of the shear thickening regime at τ_2, $\Delta\sigma_{\text{net}}/\sigma_0$ grows with time at a rate of roughly 8×10^{-5} s^{-1}. This rate further increases to 3×10^{-4} s^{-1} near the peak of thickening at τ_3. This growth of conductance over successive shear oscillation cycles would then suggest that such cyclic training sets up particularly robust contact force networks, which in turn generate robust conditions for piezoelectric charge generation that becomes more efficient over time as particles nestle into configurations optimized for shear reversal.

In Fig. 3*B*, we start from stress level τ_3 and after 3,600 s abruptly cut the oscillation strain amplitude by five orders of magnitude, thereby switching from a stress $\tau_3 = 1 \times 10^4$ Pa to $\tau_0 = 10$ Pa. Since this BTO suspension is strongly shear thinning, its viscosity η^* jumps up by two orders of magnitude (Fig.. 3 *A*, *Inset*). In this state, the system is far below the onset of shear thickening so that a stress-activated frictional force chain network can no longer be maintained and the particles reconfigure into a frictionless configuration held together by attractive forces. As Fig. 3*B* shows, this disassembly of the trained-in network is very slow and likely occurs by particle diffusion, given that the Péclet number dropped from Pe $\approx$ 5,000 to Pe = 0.01 during shear cessation (Pe $= 6\pi\eta_f a^3\gamma_0\omega/k_B T$ characterizes the ratio of advective to diffusive transport rates for a particle of diameter a in a liquid of viscosity η_f). Yet even in a partially disintegrated frictional network, oscillatory excitation with very small strain evidently still generates a piezoelectric response that shows up as clear signal in the excess conductance.

To further confirm that the measured excess ac conductance is due to a change in the stress state of individual particles during shear-induced frictional network formation, a piezo-chemical reaction was examined. Such reactions require that particles experience significant stresses, typically produced by ball milling (36, 37), ultrasound (38, 39), or electrodynamic agitation (27). By using a polymerization reaction known to be driven by mechanically activated piezochemistry, the detection of crosslinking under shear can be used as a readout to signal that sufficiently large stress on the particles has changed the local charge environment and enabled a chemical reaction in the surrounding polymeric fluid. To this end, ZnO particles are suspended in a monomer mixture of dipentaerythritol hexakis (3-mercaptopropionate) (DiPETMP) and tri(ethylene glycol) divinyl ether (TEGDE) (Fig. 4*A*) and the kinetics of the thiol-ene crosslinking reaction are observed over time. This reaction has been shown to be mediated by electrodynamic agitation of a solution containing a low concentration of ZnO particles (27). Fig. 4*B* demonstrates that oscillatory shear ($\omega = 50$ rad s^{-1} and $\gamma_0 = 80\%$) can indeed transform the initially viscous fluid into a polymerized solid. In Fig. 4*C*, the polymerization reaction

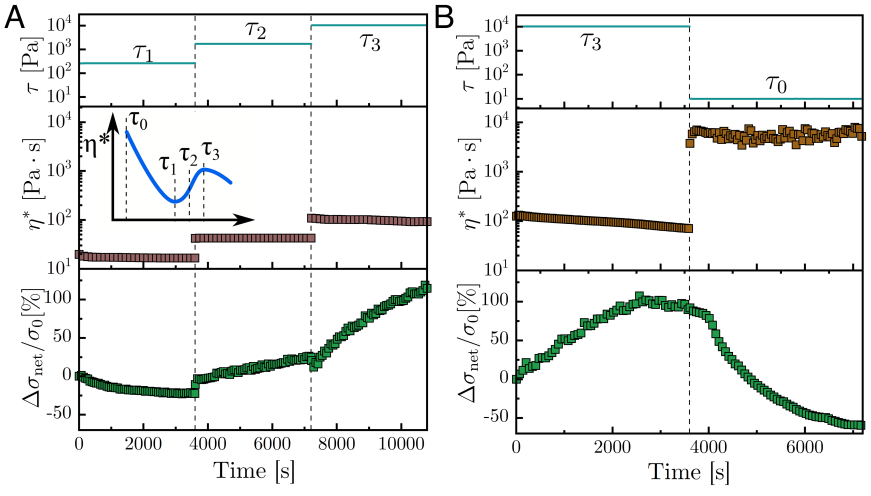

Fig. 3. Tracking the evolution of the network of stress-activated frictional contacts. Conductance measurements provide a magnified view into the evolution of the contact network after step-wise changes of the applied shear stress τ. Data shown are for a BTO suspension with $\phi = 0.46$ and taken with stress-controlled oscillatory shear at $\omega = 50$ rad/s. (*A*) Viscosity (*Middle*) and excess ac conductance (*Bottom*) in response to stress increases (*Top*) from shear thickening onset ($\tau_1 = 710$ Pa) to intermediate stress ($\tau_2 = 1710$ Pa), to stress at the peak of the shear-thickening regime ($\tau_3 = 1 \times 10^4$ Pa), as illustrated by the inset. (*B*) Viscosity (*Middle*) and excess ac conductance (*Bottom*) in response to an abrupt shear cessation (*Top*) from $\tau = \tau_3$ to a low stress τ_0 in the shear thinning regime [*Inset* to (*A*)].

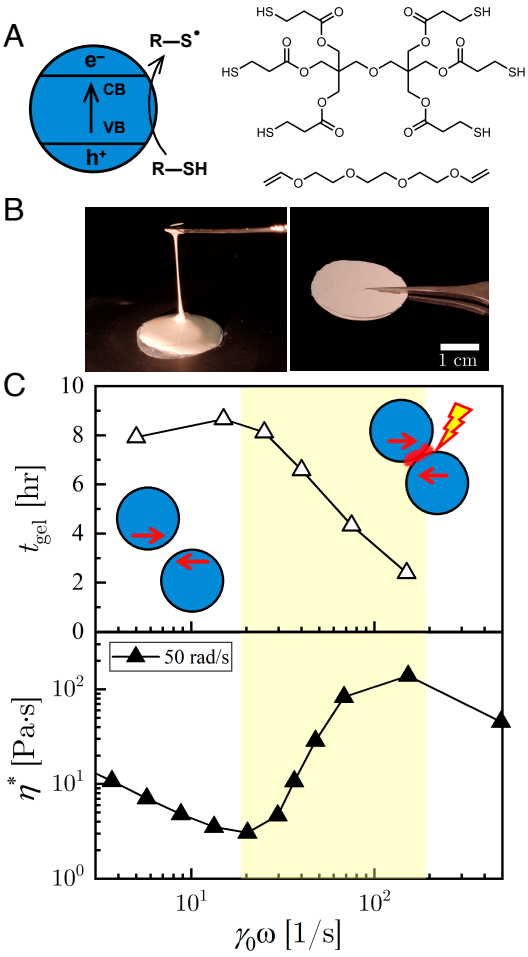

Fig. 4. In situ control of piezochemistry reaction kinetics with low-frequency oscillatory shear. (*A*) Charge generation in ZnO nanoparticles drives crosslinking in a mixture of dipentaerythritol hexakis(3-mercaptopropionate) and tri(ethylene glycol) divinyl ether. (*B*) An initially fluid-like suspension of the mixture (*Left*) is transformed into a crosslinked solid upon shear (*Right*) at $\omega = 50\,\mathrm{rad\,s^{-1}}$ and $\gamma_0 = 80\%$. (*C*) The reaction kinetics, measured by the gelation time t_{gel} (*Top*), along with complex viscosity η^* (*Bottom*) versus dynamic shear rate ($\gamma_0\omega$). The decrease in gelation time in the shear thickening regime (highlighted in yellow) demonstrates that it is possible to adjust the kinetics in situ using different shear rates. η^* was measured by strain-sweep experiments with an uncrosslinked suspension.

kinetics are tracked by measuring the gelation time t_{gel} for a 70 wt.% ZnO suspension in a DiPETMP and TEGDE mixture solution (1:3 molar ratio), using oscillatory strain of different amplitude with a fixed frequency $\omega = 50\,\mathrm{rad\,s^{-1}}$. As $\gamma_0\omega$ is increased and the onset of shear thickening is reached, t_{gel} starts to become reduced, eventually dropping by as much as a factor 4 at large dynamic shear rate $\gamma_0\omega$ (see *SI Appendix*, Fig. S5 for data with $\omega = 10\,\mathrm{rad\,s^{-1}}$). The result is a striking correlation between the onset of piezochemical reaction kinetics and the onset of shear-thickening.

In conclusion, our simultaneous measurements of viscosity and excess ac conductance, together with the observed enhancement of the reaction kinetics, provide strong experimental evidence for the emergence of networks of frictional particle–particle contacts in the shear-thickening regime of piezoelectric dense suspensions. Further evidence for frictional stress in these suspensions comes from our finding that oscillatory shear trains the particle configurations in these networks and, as highlighted by the evolution of the excess conductance, leads to structural memory. Overall, our observations demonstrate that the excess conductance in piezoelectric suspensions acts as a macroscale reporter and amplifier of very subtle, local and much more microscopic changes in the nature of the particle interactions as increased stress drives these interactions from lubricated to frictional. These findings also open up opportunities for further exploring how frictional contacts aid in the memory formation process and in the relaxation of the memory-formed state. Finally, while the piezoelectric particle suspensions studied here exhibit strong friction-induced shear thickening, by inserting a low concentration of piezoelectric particles as probe particles, it may be possible to track the onset of large local stresses also in suspensions with other particle types or where shear thickening is lubrication-dominated (40).

Materials and Methods

Sample Preparation and Characterization. Barium titanate (Stock number, US3827) and zinc oxide (Stock number, US1003M) particles were purchased from US Research Nanomaterials, Inc. and used as received. Dense suspensions were prepared by weight concentration, and the particle volume fraction was estimated using the particle density, $\rho = 5.85\ \mathrm{g/cm^3}$ for barium titanate and $\rho = 5.606\ \mathrm{g/cm^3}$ for zinc oxide. Glycerol (Fisher Scientific, Catalog Number: BP229-1) was added to the particles, and the suspensions were mixed for at least a day. The prepared suspensions were sealed with Parafilm to avoid possible water adsorption and were sonicated before use.

Particles were imaged with a scanning electron microscope (Merlin SEM, Carl Zeiss) at accelerating voltage 3 to 4 kV.

Rheology and Electrical Measurements. Rheology measurements were conducted with a Discovery HR 30 rheometer (TA Instruments). All measurements were performed with a parallel plate geometry with plate diameter 25 mm. For the conductance measurement, an LCR meter (E4980A, Keysight Technologies) was connected to both the bottom and top plate. The LCR meter was recalibrated in open- and short-circuit states before each measurement. For the conductance measurements, an ac voltage of 1 V_{rms} and frequency of 100 Hz was used. The rheometer tool gap size was fixed at $h = 0.33 \pm 0.02$ mm. Before each measurement, the sample was left unstressed for more than 10 min to remove possible generation of charges while being loaded into the rheometer. To minimize the effect of particle sedimentation, all samples were mixed prior to every measurement. Following Richardson and Zaki (41), we estimate the sedimentation velocity as $U = U_0(1-\phi)^m$, with $m \approx 5$ and $U_0 = 2\Delta\rho a^2 g/(9\eta) \approx 4 \times 10^{-10}$ m/s. Here a is the average particle radius, g is the gravitational acceleration, η is the fluid viscosity, and $\Delta\rho$ is the density difference between the particle and the suspending medium. This velocity leads to a sedimentation distance of no more than a few micrometers during a $\sim$ 20 min measurement (10 min waiting time for charge relaxation plus approximately 10 min for the combined rheology and conductance measurements). During the measurement, nitrogen gas was flowed into a custom-made trap to prevent the absorption of water from the air. All rheology measurements were performed using stress-controlled oscillatory shear.

The background noise in the ac conductance measurement in the low-shear-rate regime before shear thickening sets a threshold of $\Delta\sigma_{net}/\sigma_0 \approx 0.3\%$ with our setup for the detection of stress-induced changes in the excess conductance. Based on the simultaneously acquired viscosity data, we can associate this threshold with a corresponding lower limit for the detectable average stress level inside the suspension. For the ZnO suspensions without added salt, which had a base conductance around 20 μS, this gives a minimum detectable stress of ≈ 3,000 Pa (see *SI Appendix*, Fig. S1 for raw data). The two orders of magnitude larger base conductance for ZnO with added salt leads to a detection limit of around 300 Pa. In BTO suspensions, with a base conductance around 120 μS, the larger piezoelectric constant about 9 times that of ZnO (42) enhances the

detection of particle–particle contact stress to ≈ 100 Pa (see *SI Appendix*, Fig. S2 for raw data).

Mechanically Transduced Thiol-Ene Crosslinking Network. A 1-to-3 molar ratio mixture of dipentaerythritol hexakis(3-mercaptopropionate) (TCI, Product No. D5212) and tri(ethylene glycol) divinyl ether (Sigma-Aldrich, Product No. 329800) was prepared. ZnO particles were added to the solution and a 70 wt.% concentration suspension was prepared. The suspension was freshly prepared and sonicated for 30 s before each experiment.

To measure the storage and loss modulus during crosslinking, a cycle of large and small amplitude oscillatory shear was repeated. In each cycle, the suspension was sheared first at a large strain amplitude for 300 s to mechanically activate the thiol-ene crosslinking reaction, after which a small amplitude shear with 1% strain amplitude was applied for 30 s to measure the storage (G') and loss (G'') modulus at a fixed angular frequency (10 rad/s or 50 rad/s). The gelation time was taken as the crossover point between G' and G''.

Data, Materials, and Software Availability. All study data are included in the article and/or *SI Appendix*.

ACKNOWLEDGMENTS. We thank Grayson L. Jackson and Michael van der Naald for fruitful discussions. Support is acknowledged from the University of Chicago Materials Research Science and Engineering Center, which is supported by the NSF under award number DMR-2011854. Additional support was provided by the Army Research Laboratory under Cooperative Agreement Number W911NF-20-2-0044 and W911NF2110023 (77358SMRIP). The views and conclusions contained in this document are those of the authors and should not be interpreted as representing the official policies, either expressed or implied, of the Army Research Laboratory, or the U.S. Government. The U.S. Government is authorized to reproduce and distribute reprints for Government purposes notwithstanding any copyright notation herein. A.P.E.-K. acknowledges support from the U.S. Air Force Office of Scientific Research (AFOSR) through FA9550-18-1-0229.

Author affiliations: [a]Pritzker School of Molecular Engineering, University of Chicago, Chicago, IL 60637; [b]James Franck Institute and Department of Physics, University of Chicago, Chicago, IL 60637; [c]Department of Chemistry, University of Chicago, Chicago, IL 60637; and [d]Chemical and Engineering Sciences Division, Argonne National Laboratory, Lemont, IL 60439

1. X. Cheng, J. H. McCoy, J. N. Israelachvili, I. Cohen, Imaging the microscopic structure of shear thinning and thickening colloidal suspensions. *Science* **333**, 1276–1279 (2011).
2. C.-P. Hsu, J. Mandal, S. N. Ramakrishna, N. D. Spencer, L. Isa, Exploring the roles of roughness, friction and adhesion in discontinuous shear thickening by means of thermo-responsive particles. *Nat. Commun.* **12**, 1–10 (2021).
3. N. Y. Lin *et al.*, Hydrodynamic and contact contributions to continuous shear thickening in colloidal suspensions. *Phys. Rev. Lett.* **115**, 228304 (2015).
4. N. M. James, E. Han, R. A. L. de la Cruz, J. Jureller, H. M. Jaeger, Interparticle hydrogen bonding can elicit shear jamming in dense suspensions. *Nat. Mater.* **17**, 965–970 (2018).
5. R. Mari, R. Seto, J. F. Morris, M. M. Denn, Shear thickening, frictionless and frictional rheologies in non-Brownian suspensions. *J. Rheol.* **58**, 1693–1724 (2014).
6. A. Singh, C. Ness, R. Seto, J. J. de Pablo, H. M. Jaeger, Shear thickening and jamming of dense suspensions: The "roll" of friction. *Phys. Rev. Lett.* **124**, 248005 (2020).
7. M. Zarei, J. Aalaie, Application of shear thickening fluids in material development. *J. Market. Res.* **9**, 10411–10433 (2020).
8. E. L. Ballantyne, D. J. Little, E. D. Wetzel, Rate-activated strapping for improved retention of protective eyewear during impact. *Sports Eng.* **20**, 171–183 (2017).
9. S. Wang *et al.*, Smart wearable Kevlar-based safeguarding electronic textile with excellent sensing performance. *Soft Matter* **13**, 2483–2491 (2017).
10. S. Pradeep, M. Nabizadeh, A. R. Jacob, S. Jamali, L. C. Hsiao, Jamming distance dictates colloidal shear thickening. *Phys. Rev. Lett.* **127**, 158002 (2021).
11. J. Brujić *et al.*, 3D bulk measurements of the force distribution in a compressed emulsion system. *Faraday Discuss.* **123**, 207–220 (2003).
12. D. M. Walker *et al.*, Self-assembly in a near-frictionless granular material: Conformational structures and transitions in uniaxial cyclic compression of hydrogel spheres. *Soft Matter* **11**, 2157–2173 (2015).
13. T. S. Majmudar, R. P. Behringer, Contact force measurements and stress-induced anisotropy in granular materials. *Nature* **435**, 1079–1082 (2005).
14. A. H. Clark, A. J. Petersen, L. Kondic, R. P. Behringer, Nonlinear force propagation during granular impact. *Phys. Rev. Lett.* **114**, 144502 (2015).
15. L. Sanfratello, E. Fukushima, R. P. Behringer, Using MR elastography to image the 3D force chain structure of a quasi-static granular assembly. *Granular Matter* **11**, 1–6 (2009).
16. R. Hurley, S. Hall, J. Andrade, J. Wright, Quantifying interparticle forces and heterogeneity in 3D granular materials. *Phys. Rev. Lett.* **117**, 098005 (2016).
17. Y. Zhang *et al.*, Bioinspired elastic piezoelectric composites for high-performance mechanical energy harvesting. *J. Mater. Chem. A* **6**, 14546–14552 (2018).
18. H. S. Kim, J.-H. Kim, J. Kim, A review of piezoelectric energy harvesting based on vibration. *Int. J. Precis. Eng. Manuf.* **12**, 1129–1141 (2011).
19. M. B. Starr, J. Shi, X. Wang, Piezopotential-driven redox reactions at the surface of piezoelectric materials. *Angew. Chem. Int. Ed.* **51**, 5962–5966 (2012).
20. S. Pednekar, J. Chun, J. F. Morris, Bidisperse and polydisperse suspension rheology at large solid fraction. *J. Rheol.* **62**, 513–526 (2018).
21. E. Brown *et al.*, Generality of shear thickening in dense suspensions. *Nat. Mater.* **9**, 220–224 (2010).
22. E. Brown *et al.*, Shear thickening and jamming in densely packed suspensions of different particle shapes. *Phys. Rev. E* **84**, 031408 (2011).
23. N. M. James, H. Xue, M. Goyal, H. M. Jaeger, Controlling shear jamming in dense suspensions via the particle aspect ratio. *Soft Matter* **15**, 3649–3654 (2019).
24. M. Desmond, N. Mavrogiannis, Z. Gagnon, Maxwell-Wagner polarization and frequency-dependent injection at aqueous electrical interfaces. *Phys. Rev. Lett.* **109**, 187602 (2012).
25. S. Jamali, J. F. Brady, Alternative frictional model for discontinuous shear thickening of dense suspensions: Hydrodynamics. *Phys. Rev. Lett.* **123**, 138002 (2019).
26. M. Youssry *et al.*, Non-aqueous carbon black suspensions for lithium-based redox flow batteries: Rheology and simultaneous rheo-electrical behavior. *Phys. Chem. Chem. Phys.* **15**, 14476–14486 (2013).
27. Z. Wang *et al.*, Bio-inspired mechanically adaptive materials through vibration-induced crosslinking. *Nat. Mater.* **20**, 869–874 (2021).
28. A. Singh, S. Pednekar, J. Chun, M. M. Denn, J. F. Morris, From yielding to shear jamming in a cohesive frictional suspension. *Phys. Rev. Lett.* **122**, 098004 (2019).
29. D. Bi, J. Zhang, B. Chakraborty, R. P. Behringer, Jamming by shear. *Nature* **480**, 355–358 (2011).
30. R. Seto, R. Mari, J. F. Morris, M. M. Denn, Discontinuous shear thickening of frictional hard-sphere suspensions. *Phys. Rev. Lett.* **111**, 218301 (2013).
31. M. D. Haw, W. C. K. Poon, P. N. Pusey, P. Hebraud, F. Lequeux, Colloidal glasses under shear strain. *Phys. Rev. E* **58**, 4673 (1998).
32. J. R. Royer, P. M. Chaikin, Precisely cyclic sand: Self-organization of periodically sheared frictional grains. *Proc. Natl. Acad. Sci. U.S.A.* **112**, 49–53 (2015).
33. C. W. Lindeman, S. R. Nagel, Multiple memory formation in glassy landscapes. *Sci. Adv.* **7**, eabg7133 (2021).
34. N. C. Keim, S. R. Nagel, Generic transient memory formation in disordered systems with noise. *Phys. Rev. Lett.* **107**, 010603 (2011).
35. L. Corte, P. M. Chaikin, J. P. Gollub, D. J. Pine, Random organization in periodically driven systems. *Nat. Phys.* **4**, 420–424 (2008).
36. K. Kubota, Y. Pang, A. Miura, H. Ito, Redox reactions of small organic molecules using ball milling and piezoelectric materials. *Science* **366**, 1500–1504 (2019).
37. C. Schumacher, J. G. Hernández, C. Bolm, Electro-mechanochemical atom transfer radical cyclizations using piezoelectric $BaTiO_3$. *Angew. Chem. Int. Ed.* **59**, 16357–16360 (2020).
38. H. Mohapatra, M. Kleiman, A. P. Esser-Kahn, Mechanically controlled radical polymerization initiated by ultrasound. *Nat. Chem.* **9**, 135–139 (2017).
39. H. Mohapatra *et al.*, Ultrasound promoted step-growth polymerization and polymer crosslinking via copper catalyzed azide-alkyne "click" reaction. *Angew. Chem. Int. Ed.* **57**, 11208–11212 (2018).
40. Y.-F. Lee *et al.*, Microstructure and rheology of shear-thickening colloidal suspensions with varying interparticle friction: Comparison of experiment with theory and simulation models. *Phys. Fluids* **33**, 033316 (2021).
41. J. F. Richardson, W. N. Zaki, Sedimentation and fluidisation. Part 1. *Trans. Inst. Chem. Eng.* **32**, 35–53 (1954).
42. M. B. Starr, X. Wang, Fundamental analysis of piezocatalysis process on the surfaces of strained piezoelectric materials. *Sci. Rep.* **3**, 2160 (2013).